Communication

An Explicit Time Marching Scheme for Efficient Solution of the Magnetic Field Integral Equation at Low Frequencies

Rui Chen, Sadeed B. Sayed, H. Arda Ulku, and Hakan Bagci

***Abstract*— An explicit marching-on-in-time (MOT) scheme to efficiently solve the time-domain magnetic field integral equation (TD-MFIE) with a large time step size (under a low-frequency excitation) is developed. The proposed scheme spatially expands the current using high-order nodal functions defined on curvilinear triangles discretizing the scatterer surface. Applying Nyström discretization, which uses this expansion, to the TD-MFIE, which is written as an ordinary differential equation (ODE) by separating self-term contribution, yields a system of ODEs in unknown time-dependent expansion coefficients. A predictor–corrector method is used to integrate this system for the samples of these coefficients. Since the Gram matrix arising from the Nyström discretization is a block-diagonal, the resulting MOT scheme replaces the matrix "inversion" required at each time step by a product of the inverse block-diagonal Gram matrix and the right-hand side vector. It is shown that, on the convergence of the corrector updates, this explicit MOT scheme produces the same solution as its implicit counterpart and is faster for large time step sizes.**

***Index Terms*— Magnetic field integral equation (MFIE), marching-on-in-time (MOT), Nyström method, predictor–corrector scheme.**

I. Introduction

Transient electromagnetic scattering from perfect electrically conducting (PEC) objects can be analyzed by solving time-domain surface integral equations (TD-SIEs) [1]–[18]. A TD-SIE for a PEC scatterer is often constructed by enforcing the electric and magnetic field boundary conditions on the scatterer surface. These boundary conditions are expressed in terms of the known incident field and the scattered field; representing the latter as a space-time integral of the unknown current induced on the scatterer surface yields the electric field integral equation (EFIE) or the magnetic field integral equation (MFIE) (depending on the type of the field used). Furthermore, the combined field integral equation (CFIE) can be obtained by linearly combining the (rotated) EFIE and the MFIE.

One of the prevalent methods developed for solving TD-SIEs is the marching-on-in-time (MOT) scheme [10]–[16]. The classical MOT scheme expands the unknown current induced on the scatterer surface using the Rao–Wilton–Glisson (RWG) basis functions [19] in space and piecewise Lagrange polynomials [3], [13], [14] in time. This expansion is inserted into the TD-SIE, and the resulting equation is Galerkin-tested in space and point-tested in time, yielding a lower triangular matrix system in unknown expansion coefficients. Applying the backward substitution to this matrix system results in a time-marching algorithm, where a reduced system of equations known as the MOT system is solved at every time step for the unknown coefficients associated with only that time step. The right-hand side of the MOT system consists of the incident and scattered fields tested at the same time step. After the solution, the coefficients, which are now known, are used for computing the tested scattered field at the next step. This process is repeated until all the expansion coefficients at all the time steps are computed.

The time step size of the MOT scheme described above is selected as $\Delta t = 1/(\alpha f_{\max})$, where $f_{\max}$ is the maximum frequency of the incident field, and α is an oversampling coefficient. For high-frequency excitations, Δt is small, and the MOT system is sparse. Consequently, the computation of the tested scattered field on the right-hand side of the MOT system is more costly than its solution (which is often done using an iterative solver). This computation is often accelerated using (multilevel) plane-wave time-domain (PWTD) algorithms [10]–[13] or fast Fourier transformation (FFT)-based schemes [14]–[16]. For low-frequency excitations, Δt is large and the MOT system is dense (even full), and the computational cost of solving this system becomes larger than that of computing the tested scattered field on the right-hand side.

In [8], a quasi-explicit MOT scheme, which does not suffer from this drawback, has been developed to solve the TD-MFIE. This scheme expresses the TD-MFIE as an ordinary differential equation (ODE) that relates the current to its temporal derivative. Discretizing this ODE using RWG basis and testing functions [19] yields a system of ODEs in time-dependent expansion coefficients of the RWG basis functions. Integrating this system in time provides the samples of these coefficients. This MOT scheme avoids solving a dense matrix system but still requires the solution of a sparse Gram matrix system at each time step.

This sparse matrix inversion required at every step can be eliminated if a spatial discretization scheme, which does not use basis functions defined over two mesh elements, is used. Indeed, in [20], an MOT scheme that makes use of this idea is used to solve the time-domain integral equations of acoustics. In this work, this scheme is extended to solve the TD-MFIE efficiently when Δt is large. The current is spatially expanded using high-order nodal interpolation functions defined on curvilinear triangular patches. Applying Nyström discretization, which uses this expansion, converts the ODE form of the TD-MFIE into a system of ODEs in time-dependent expansion coefficients. Then, this system is integrated using a predictor–corrector $(\mathrm{PE(CE)}^m)$ scheme to yield the samples of these coefficients. The Gram matrix arising from the Nyström discretization is block-diagonal (with 2×2 blocks), and its inverse is constructed very efficiently from the inverse of these blocks at the beginning of time integration. Therefore, the matrix inversion required at every time step is replaced by a block matrix and vector product. This explicit MOT scheme maintains its stability even when using Δt as large as that would be used by its implicit counterpart (traditional MOT scheme, where RWG-based discretization is replaced by Nyström discretization [18]) and is significantly faster for

Manuscript received April 16, 2020; revised June 18, 2020; accepted July 7, 2020. Date of publication July 27, 2020; date of current version February 3, 2021. This work was supported by the King Abdullah University of Science and Technology (KAUST) Office of Sponsored Research (OSR) under Award No 2016-CRG5-2953. *(Corresponding author: Rui Chen.)*

Rui Chen and Hakan Bagci are with the Division of Computer, Electrical, and Mathematical Science and Engineering, King Abdullah University of Science and Technology (KAUST), Thuwal 23955-6900, Saudi Arabia (e-mail: rui.chen@kaust.edu.sa; hakan.bagci@kaust.edu.sa).

Sadeed B. Sayed was with the Division of Computer, Electrical, and Mathematical Science and Engineering, King Abdullah University of Science and Technology (KAUST), Thuwal 23955-6900, Saudi Arabia. He is now with the School of Electrical and Electronic Engineering, Nanyang Technological University, Singapore (e-mail: sadeed.sayed@ntu.edu.sg).

H. Arda Ulku is with the Department of Electronics Engineering, Gebze Technical University, 41400 Gebze, Turkey (e-mail: haulku@gtu.edu.tr).

Color versions of one or more of the figures in this communication are available online at https://ieeexplore.ieee.org.

Digital Object Identifier 10.1109/TAP.2020.3010997

large Δt. In addition, it is shown that when the orders of the temporal basis function of the implicit solver and the PE(CE)^m scheme of the explicit solver are the same, both the solvers produce the same solution on convergence of the corrector updates.

II. Formulation

A. TD-MFIE

Let S denote the surface of a PEC object residing in an unbounded homogeneous medium with permittivity ε and permeability μ. An electromagnetic wave with magnetic field $\mathbf{H}^{\mathrm{i}}(\mathbf{r},t)$ that is band-limited to $f_{\max}$ is incident on the object. An electric current $\mathbf{J}(\mathbf{r},t)$ is induced on S and generates a scattered magnetic field $\mathbf{H}^{\mathrm{s}}(\mathbf{r},t)$ as

$$\mathbf{H}^{\mathrm{s}}(\mathbf{r},t)=\int_S \nabla\times\frac{\mathbf{J}(\mathbf{r}',t')}{4\pi R}ds'. \tag{1}$$

Here, $t'=t-R/c$ is the retarded time, $R=|\mathbf{r}-\mathbf{r}'|$ is the distance between the points $\mathbf{r}$ and $\mathbf{r}'$, and $c=1/\sqrt{\mu\varepsilon}$ is the speed of light. Inserting (1) into the temporal derivative of the magnetic-field boundary condition on S, i.e., $\partial_t\mathbf{J}(\mathbf{r},t)=\partial_t\hat{\mathbf{n}}(\mathbf{r})\times[\mathbf{H}^{\mathrm{i}}(\mathbf{r},t)+\mathbf{H}^{\mathrm{s}}(\mathbf{r},t)]$, yields the temporal derivative form of the TD-MFIE as [8]

$$\frac{1}{2}\partial_t\mathbf{J}(\mathbf{r},t)=\hat{\mathbf{n}}(\mathbf{r})\times\partial_t\mathbf{H}^{\mathrm{i}}(\mathbf{r},t)+\hat{\mathbf{n}}(\mathbf{r})\times\int_S\nabla\times\frac{\partial_t\mathbf{J}(\mathbf{r}',t')}{4\pi R}ds'. \tag{2}$$

Here, $\hat{\mathbf{n}}(\mathbf{r})$ is the unit normal vector pointing outward from S at $\mathbf{r}$.

B. Discretization

To numerically solve (2), $\mathbf{J}(\mathbf{r},t)$ is expanded in space using high-order Lagrange polynomial interpolation functions as [21]

$$\mathbf{J}(\mathbf{r},t)=\sum_{p=1}^{N_{\mathrm{p}}}\sum_{i=1}^{N_{\mathrm{n}}}\left[\{\mathbf{I}(t)\}_{ip}^{\mathrm{u}}\mathbf{u}(\mathbf{r})+\{\mathbf{I}(t)\}_{ip}^{\mathrm{v}}\mathbf{v}(\mathbf{r})\right]\vartheta^{-1}(\mathbf{r})\ell_{ip}(\mathbf{r}). \tag{3}$$

Here, N_{p} and N_{n} are the numbers of the curvilinear triangular patches discretizing S and the interpolation nodes on each patch, respectively, $\ell_{ip}(\mathbf{r})$ represents the Lagrange interpolation function defined at node $\mathbf{r}_{ip}$ (node i on patch p), $\vartheta(\mathbf{r})$ is the Jacobian of the transformation that maps the patch description in the Cartesian coordinate system to the right triangle defined by variable pair (u,v), vectors $\mathbf{u}(\mathbf{r})=\partial_u\mathbf{r}$ and $\mathbf{v}(\mathbf{r})=\partial_v\mathbf{r}$ are tangential to S at $\mathbf{r}$, and $\{\mathbf{I}(t)\}_{ip}^{\mathrm{u}}$ and $\{\mathbf{I}(t)\}_{ip}^{\mathrm{v}}$ are the time-dependent unknown expansion coefficients of $\mathbf{J}(\mathbf{r}_{ip},t)$'s components along the directions of $\mathbf{u}(\mathbf{r}_{ip})$ and $\mathbf{v}(\mathbf{r}_{ip})$, respectively. To account for the time retardation t' in (2), $\{\mathbf{I}(t)\}_{ip}^{\mathrm{b}}$ and $\mathrm{b}\in\{\mathrm{u},\mathrm{v}\}$ are expanded using piecewise Lagrange polynomial interpolation functions as [3], [13], [14]

$$\{\mathbf{I}(t)\}_{ip}^{\mathrm{b}}=\sum_{l=1}^{N_{\mathrm{t}}}I_l|_{ip}^{\mathrm{b}}T(t-l\Delta t). \tag{4}$$

Here, $I_l|_{ip}^{\mathrm{b}}=\{\mathbf{I}(l\Delta t)\}_{ip}^{\mathrm{b}}$, $\mathrm{b}\in\{\mathrm{u},\mathrm{v}\}$, $T(t)$ is constructed using piecewise Lagrange polynomials, and N_{t} is the number of time steps.

C. Explicit MOT Scheme (E-MOT)

Substituting (3) into (2) and spatially testing with $\mathbf{u}(\mathbf{r}_{jq})$ and $\mathbf{v}(\mathbf{r}_{jq})$, $j=1,\ldots,N_{\mathrm{n}}$, $q=1,\ldots,N_{\mathrm{p}}$ yield a time-dependent semidiscrete system of ODEs. This system has to be sampled at times $t=h\Delta t$ to carry out the time integration using a PE(CE)^m-type scheme [8], [20], [22]. Consequently, one has to use temporal interpolation on $\{\mathbf{I}(t')\}_{ip}^{\mathrm{b}}$, $\mathrm{b}\in\{\mathrm{u},\mathrm{v}\}$. This is done by using (4), which leads to a fully discretized linear system as

$$\mathbf{G}\dot{\mathbf{I}}_h=\mathbf{V}_h^{\mathrm{i}}-\sum_{l=1}^{h}\mathbf{Z}_{h-l}^{\mathrm{exp}}\mathbf{I}_l,\quad h=1,\ldots,N_{\mathrm{t}}. \tag{5}$$

Here, the block-diagonal Gram matrix $\mathbf{G}$ is given by (6) at the bottom of the next page, where its entries are

$$G|_{jq,ip}^{\mathrm{ab}}=\frac{1}{2}\mathbf{a}(\mathbf{r}_{jq})\cdot\mathbf{b}(\mathbf{r}_{ip})\vartheta^{-1}(\mathbf{r}_{ip}) \tag{7}$$

$\mathrm{a},\mathrm{b}\in\{\mathrm{u},\mathrm{v}\}$, $\mathbf{a},\mathbf{b}\in\{\mathbf{u},\mathbf{v}\}$, and the E-MOT matrices $\mathbf{Z}_{h-l}^{\mathrm{exp}}$ are given by (8) at the bottom of the next page, where their entries are

$$\begin{aligned}Z_{h-l}^{\mathrm{exp}}|_{jq,ip}^{\mathrm{ab}}=\mathbf{a}(\mathbf{r}_{jq})\cdot\hat{\mathbf{n}}(\mathbf{r}_{jq})\times\int_{S_p}\vartheta^{-1}(\mathbf{r}')\ell_{ip}(\mathbf{r}')\\ \times\frac{\mathbf{R}}{4\pi R^3}\left[\partial_tT(t)+\frac{R}{c}\partial_t^2T(t)\right]_{t=(h-l)\Delta t-R/c}\\ \times\mathbf{b}(\mathbf{r}')ds'\end{aligned} \tag{9}$$

where S_p is the support of patch p, $\mathbf{R}=\mathbf{r}_{jq}-\mathbf{r}'$, $R=|\mathbf{r}_{jq}-\mathbf{r}'|$, and the tested excitation vector $\mathbf{V}_h^{\mathrm{i}}$ are given by

$$\mathbf{V}_h^{\mathrm{i}}=\left[V_h^{\mathrm{i}}|_{11}^{\mathrm{u}},\ V_h^{\mathrm{i}}|_{11}^{\mathrm{v}},\ V_h^{\mathrm{i}}|_{21}^{\mathrm{u}},\ V_h^{\mathrm{i}}|_{21}^{\mathrm{v}},\ldots,V_h^{\mathrm{i}}|_{N_{\mathrm{i}}N_{\mathrm{p}}}^{\mathrm{u}},\ V_h^{\mathrm{i}}|_{N_{\mathrm{i}}N_{\mathrm{p}}}^{\mathrm{v}}\right]^T$$

with entries $V_h^{\mathrm{i}}|_{jq}^{\mathrm{a}}=\mathbf{a}(\mathbf{r}_{jq})\cdot\hat{\mathbf{n}}(\mathbf{r}_{jq})\times\partial_t\mathbf{H}^{\mathrm{i}}(\mathbf{r}_{jq},h\Delta t)$, and the unknown coefficient vector $\mathbf{I}_l$ are given by

$$\mathbf{I}_l=\left[I_l|_{11}^{\mathrm{u}},\ I_l|_{11}^{\mathrm{v}},\ I_l|_{21}^{\mathrm{u}},\ I_l|_{21}^{\mathrm{v}},\ldots,I_l|_{N_{\mathrm{i}}N_{\mathrm{p}}}^{\mathrm{u}},\ I_l|_{N_{\mathrm{i}}N_{\mathrm{p}}}^{\mathrm{v}}\right]^T$$

and $\dot{\mathbf{I}}_h$ store samples of the time derivative of the coefficients as

$$\dot{\mathbf{I}}_h=\left[\dot{I}_h|_{11}^{\mathrm{u}},\ \dot{I}_h|_{11}^{\mathrm{v}},\ \dot{I}_h|_{21}^{\mathrm{u}},\ \dot{I}_h|_{21}^{\mathrm{v}},\cdots\dot{I}_h|_{N_{\mathrm{i}}N_{\mathrm{p}}}^{\mathrm{u}},\ \dot{I}_h|_{N_{\mathrm{i}}N_{\mathrm{p}}}^{\mathrm{v}}\right]^T$$

with $\dot{I}_h|_{ip}^{\mathrm{b}}=\{\partial_t\mathbf{I}(h\Delta t)\}_{ip}^{\mathrm{b}}$. Note that the weak singularity of the integral in (9) is canceled using the Duffy transformation [23] to permit its numerical evaluation.

A PE(CE)^m scheme is used to integrate the ODE system (5) to yield $\mathbf{I}_h$, $h=1,\ldots,N_{\mathrm{t}}$ [8], [20], [22]. The steps of this scheme are briefly summarized as follows:

---

0) Compute $\mathbf{G}^{-1}$

Loop over $h=1,\ldots,N_{\mathrm{t}}$

1) Compute the part of right-hand side of (5) that does not change within time step h

$$\mathbf{V}_h^{\mathrm{fix}}=\mathbf{V}_h^{\mathrm{i}}-\sum_{l=1}^{h-1}\mathbf{Z}_{h-l}^{\mathrm{exp}}\mathbf{I}_l. \tag{10}$$

2) Predict $\mathbf{I}_h$ using $\mathbf{I}_l$ and $\dot{\mathbf{I}}_l$

$$\mathbf{I}_h=\sum_{k=1}^{K}[\{\mathbf{p}\}_k\mathbf{I}_{h-1+k-K}+\{\mathbf{p}\}_{K+k}\dot{\mathbf{I}}_{h-1+k-K}]. \tag{11}$$

3) Evaluate $\dot{\mathbf{I}}_h$ using $\mathbf{V}_h^{\mathrm{fix}}$ and the predicted $\mathbf{I}_h$

$$\dot{\mathbf{I}}_h=\mathbf{G}^{-1}\left(\mathbf{V}_h^{\mathrm{fix}}-\mathbf{Z}_0^{\mathrm{exp}}\mathbf{I}_h\right). \tag{12}$$

4) Set $\dot{\mathbf{I}}_h^{(0)}=\dot{\mathbf{I}}_h$ and start (CE)^m updates

Loop over $n=1,\ldots,m$ (until convergence)

4.1) Correct $\mathbf{I}_h^{(n)}$ using $\dot{\mathbf{I}}_h^{(n-1)}$, $\mathbf{I}_l$ and $\dot{\mathbf{I}}_l$

$$\begin{aligned}\mathbf{I}_h^{(n)}=\sum_{k=1}^{K}[\{\mathbf{c}\}_k\mathbf{I}_{h-1+k-K}+\{\mathbf{c}\}_{K+k}\dot{\mathbf{I}}_{h-1+k-K}]\\ +\{\mathbf{c}\}_{2K+1}\dot{\mathbf{I}}_h^{(n-1)}.\end{aligned} \tag{13}$$

4.2) Evaluate $\dot{\mathbf{I}}_h^{(n)}$ using $\mathbf{V}_h^{\mathrm{fix}}$ and the corrected $\mathbf{I}_h^{(n)}$

$$\dot{\mathbf{I}}_h^{(n)}=\mathbf{G}^{-1}\left(\mathbf{V}_h^{\mathrm{fix}}-\mathbf{Z}_0^{\mathrm{exp}}\mathbf{I}_h^{(n)}\right). \tag{14}$$

4.3) Check convergence $\|\mathbf{I}_h^{(n)}-\mathbf{I}_h^{(n-1)}\|<\chi^{\mathrm{PECE}}$, where χ^{PECE} is a threshold parameter.

End loop over n

5): Once convergence is achieved, e.g., at iteration m, set $\mathbf{I}_h=\mathbf{I}_h^{(m)}$ and $\dot{\mathbf{I}}_h=\dot{\mathbf{I}}_h^{(m)}$.

End loop over h.

Here, vectors $\mathbf{p}$ and $\mathbf{c}$ store the predictor and corrector coefficients, which are obtained using polynomial interpolation/extrapolation on the temporal samples of the solution (e.g., Adam–Moulton, Adam–Bashforth, and backward difference methods [24]), respectively. The Gram matrix $\mathbf{G}$ does not depend on Δt and is block-diagonal with 2×2 blocks. Therefore, $\mathbf{G}^{-1}$ is constructed very efficiently using

the inverses of $\mathbf{G}$'s blocks and is stored before the time marching starts. Since $\mathbf{G}^{-1}$ is also block diagonal, the solutions of matrix systems in (12) and (14) are done by simply multiplying $\mathbf{G}^{-1}$ with the right-hand side vector. At the start of time marching, it is assumed that $\mathbf{I}_l = \mathbf{0}$ and $\dot{\mathbf{I}}_l = \mathbf{0}$, for $l = 1-K, \ldots, 0$. This assumption does not introduce any significant errors in the solution since $\mathbf{H}^{\mathrm{i}}(\mathbf{r}, t)$ is vanishingly small for $t \leq 0$, $\forall \mathbf{r} \in S$ and bandlimited to $f_{\max}$.

D. Implicit MOT Scheme (I-MOT)

Substituting (3) and (4) into (2) and testing with $\mathbf{u}(\mathbf{r}_{jq})$ and $\mathbf{v}(\mathbf{r}_{jq})$, $j = 1, \ldots, N_{\mathrm{n}}$, $q = 1, \ldots, N_{\mathrm{p}}$ at times $t = h\Delta t$, $h = 1, \ldots, N_{\mathrm{t}}$ yield the I-MOT system as [18]

$$\mathbf{Z}_0^{\mathrm{imp}}\mathbf{I}_h = \mathbf{V}_h^{\mathrm{i}} - \sum_{l=1}^{h-1} \mathbf{Z}_{h-l}^{\mathrm{imp}}\mathbf{I}_l, \quad h = 1, \ldots, N_{\mathrm{t}}. \tag{15}$$

Here, $\mathbf{I}_l$ and $\mathbf{V}_h^{\mathrm{i}}$ are the same as those in (5), and the implicit MOT matrices $\mathbf{Z}_{h-l}^{\mathrm{imp}}$ are given by

$$\mathbf{Z}_{h-l}^{\mathrm{imp}} = \mathbf{G}\partial_t T(t)|_{t=(h-l)\Delta t} + \mathbf{Z}_{h-l}^{\mathrm{exp}}. \tag{16}$$

The unknown vectors $\mathbf{I}_h$, $h = 1, \ldots, N_{\mathrm{t}}$ are computed recursively using a time-marching scheme. First, at $t = \Delta t$, $\mathbf{I}_1$ is obtained by solving $\mathbf{Z}_0^{\mathrm{imp}}\mathbf{I}_1 = \mathbf{V}_1^{\mathrm{i}}$ [$h = 1$ in (15)]. Then, at $t = 2\Delta t$, $\mathbf{I}_2$ is found by solving $\mathbf{Z}_0^{\mathrm{imp}}\mathbf{I}_2 = \mathbf{V}_2^{\mathrm{i}} - \mathbf{Z}_1^{\mathrm{imp}}\mathbf{I}_1$ [$h = 2$ in (15)]. Next, at $t = 3\Delta t$, $\mathbf{I}_3$ is computed by solving $\mathbf{Z}_0^{\mathrm{imp}}\mathbf{I}_3 = \mathbf{V}_3^{\mathrm{i}} - \mathbf{Z}_2^{\mathrm{imp}}\mathbf{I}_1 - \mathbf{Z}_1^{\mathrm{imp}}\mathbf{I}_2$ [$h = 3$ in (15)] and so on. During this time-marching scheme, the solution of the MOT system (15) required at each time step is obtained using the transpose-free quasi-minimal residual (TFQMR) scheme [25]. This iterative solver is stopped when $\|\mathbf{I}_h^{(n)} - \mathbf{I}_h^{(n-1)}\| < \chi^{\mathrm{TFQMR}}$, where $\mathbf{I}_h^{(n)}$ and χ^{TFQMR} represent the solution vector at iteration n and a threshold parameter, respectively.

E. Comparison of Implicit and Explicit Solutions

In this section, it is shown that, when both I-MOT and E-MOT use the same Δt, the corrector updates of E-MOT produce the same result as the iterative solution of the I-MOT system on convergence if $T(t)$ (consisting of piecewise Lagrange polynomials) has the same order as the Lagrange polynomial interpolation used to derive the corrector coefficients $\mathbf{c}$. This is best demonstrated by an example. Assume that $\mathbf{c}$ is obtained using a third-order backward difference method [24], which leads to

$$\mathbf{I}_h - \frac{18}{11}\mathbf{I}_{h-1} + \frac{9}{11}\mathbf{I}_{h-2} - \frac{2}{11}\mathbf{I}_{h-3} = \frac{6}{11}\Delta t\dot{\mathbf{I}}_h. \tag{17}$$

Assuming that the corrector updates have converged, inserting (17) into (5) yields the matrix system

$$\frac{11}{6\Delta t}\mathbf{G}\mathbf{I}_h - \frac{3}{\Delta t}\mathbf{G}\mathbf{I}_{h-1} + \frac{3}{2\Delta t}\mathbf{G}\mathbf{I}_{h-2} - \frac{1}{3\Delta t}\mathbf{G}\mathbf{I}_{h-3} = \mathbf{V}_h^{\mathrm{i}} - \sum_{l=1}^{h} \mathbf{Z}_{h-l}^{\mathrm{exp}}\mathbf{I}_l, \quad h = 1, \ldots, N_{\mathrm{t}} \tag{18}$$

whose solution for $\mathbf{I}_h$ should be equal to the result of the corrector updates. Merging the "past/history" terms with $\mathbf{I}_{h-3}$, $\mathbf{I}_{h-2}$, and $\mathbf{I}_{h-1}$ to the right-hand side of (18) and collecting the "instantaneous/current" terms with $\mathbf{I}_h$ on the left-hand side yield

$$\tilde{\mathbf{Z}}_0^{\mathrm{exp}}\mathbf{I}_h = \mathbf{V}_h^{\mathrm{i}} - \sum_{l=1}^{h-1} \tilde{\mathbf{Z}}_{h-l}^{\mathrm{exp}}\mathbf{I}_l, \quad h = 1, \ldots, N_{\mathrm{t}} \tag{19}$$

where $\tilde{\mathbf{Z}}_0^{\mathrm{exp}} = 11/(6\Delta t)\mathbf{G} + \mathbf{Z}_0^{\mathrm{exp}}$, $\tilde{\mathbf{Z}}_1^{\mathrm{exp}} = -3/(\Delta t)\mathbf{G} + \mathbf{Z}_1^{\mathrm{exp}}$, $\tilde{\mathbf{Z}}_2^{\mathrm{exp}} = 3/(2\Delta t)\mathbf{G} + \mathbf{Z}_2^{\mathrm{exp}}$, $\tilde{\mathbf{Z}}_3^{\mathrm{exp}} = -1/(3\Delta t)\mathbf{G} + \mathbf{Z}_3^{\mathrm{exp}}$, and $\tilde{\mathbf{Z}}_{h-l}^{\mathrm{exp}} = \mathbf{Z}_{h-l}^{\mathrm{exp}}$, $l = 1, \ldots, h-4$.

Assume that $T(t)$ is constructed using third-order Lagrange polynomials [13] [the same order as the one used for backward difference in (17)], then $\partial_t T(t)|_{t=0} = 11/(6\Delta t)$, $\partial_t T(t)|_{t=\Delta t} = -3/\Delta t$, $\partial_t T(t)|_{t=2\Delta t} = 3/(2\Delta t)$, and $\partial_t T(t)|_{t=3\Delta t} = -1/(3\Delta t)$. Inserting these expressions in (16) yields $\mathbf{Z}_0^{\mathrm{imp}} = 11/(6\Delta t)\mathbf{G} + \mathbf{Z}_0^{\mathrm{exp}}$, $\mathbf{Z}_1^{\mathrm{imp}} = -3/(\Delta t)\mathbf{G} + \mathbf{Z}_1^{\mathrm{exp}}$, $\mathbf{Z}_2^{\mathrm{imp}} = 3/(2\Delta t)\mathbf{G} + \mathbf{Z}_2^{\mathrm{exp}}$, $\mathbf{Z}_3^{\mathrm{imp}} = -1/(3\Delta t)\mathbf{G} + \mathbf{Z}_3^{\mathrm{exp}}$, and $\mathbf{Z}_{h-l}^{\mathrm{imp}} = \mathbf{Z}_{h-l}^{\mathrm{exp}}$, $l = 1, \ldots, h-4$, which demonstrates that the system in (19) is the same as the I-MOT system. Then, one can argue that, on convergence, the corrector updates produce the same result as the iterative solution of the I-MOT system. This statement is verified by the numerical examples in Section III. Note that the numerical results also show that E-MOT can use the same Δt as I-MOT without sacrificing the stability of the solution.

F. Computational Complexity Analysis

Before comparing the computational complexity of I-MOT and E-MOT, three observations are noted.

$$\mathbf{G} = \begin{bmatrix} G|^{\mathrm{uu}}_{11,11} & G|^{\mathrm{uv}}_{11,11} & & & & & \\ G|^{\mathrm{vu}}_{11,11} & G|^{\mathrm{vv}}_{11,11} & & & & & \\ & & G|^{\mathrm{uu}}_{21,21} & G|^{\mathrm{uv}}_{21,21} & & & \\ & & G|^{\mathrm{vu}}_{21,21} & G|^{\mathrm{vv}}_{21,21} & & & \\ & & & & \ddots & & \\ & & & & & \ddots & \\ & & & & & & G|^{\mathrm{uu}}_{N_{\mathrm{n}}N_{\mathrm{p}},N_{\mathrm{n}}N_{\mathrm{p}}} \quad G|^{\mathrm{uv}}_{N_{\mathrm{n}}N_{\mathrm{p}},N_{\mathrm{n}}N_{\mathrm{p}}} \\ & & & & & & G|^{\mathrm{vu}}_{N_{\mathrm{n}}N_{\mathrm{p}},N_{\mathrm{n}}N_{\mathrm{p}}} \quad G|^{\mathrm{vv}}_{N_{\mathrm{n}}N_{\mathrm{p}},N_{\mathrm{n}}N_{\mathrm{p}}} \end{bmatrix} \tag{6}$$

$$\mathbf{Z}_{h-l}^{\mathrm{exp}} = \begin{bmatrix} Z_{h-l}^{\mathrm{exp}}|^{\mathrm{uu}}_{11,11} & Z_{h-l}^{\mathrm{exp}}|^{\mathrm{uv}}_{11,11} & Z_{h-l}^{\mathrm{exp}}|^{\mathrm{uu}}_{11,21} & Z_{h-l}^{\mathrm{exp}}|^{\mathrm{uv}}_{11,21} & \cdots & \cdots & Z_{h-l}^{\mathrm{exp}}|^{\mathrm{uu}}_{11,N_{\mathrm{n}}N_{\mathrm{p}}} & Z_{h-l}^{\mathrm{exp}}|^{\mathrm{uv}}_{11,N_{\mathrm{n}}N_{\mathrm{p}}} \\ Z_{h-l}^{\mathrm{exp}}|^{\mathrm{vu}}_{11,11} & Z_{h-l}^{\mathrm{exp}}|^{\mathrm{vv}}_{11,11} & Z_{h-l}^{\mathrm{exp}}|^{\mathrm{vu}}_{11,21} & Z_{h-l}^{\mathrm{exp}}|^{\mathrm{vv}}_{11,21} & \cdots & \cdots & Z_{h-l}^{\mathrm{exp}}|^{\mathrm{vu}}_{11,N_{\mathrm{n}}N_{\mathrm{p}}} & Z_{h-l}^{\mathrm{exp}}|^{\mathrm{vv}}_{11,N_{\mathrm{n}}N_{\mathrm{p}}} \\ Z_{h-l}^{\mathrm{exp}}|^{\mathrm{uu}}_{21,11} & Z_{h-l}^{\mathrm{exp}}|^{\mathrm{uv}}_{21,11} & Z_{h-l}^{\mathrm{exp}}|^{\mathrm{uu}}_{21,21} & Z_{h-l}^{\mathrm{exp}}|^{\mathrm{uv}}_{21,21} & \cdots & \cdots & Z_{h-l}^{\mathrm{exp}}|^{\mathrm{uu}}_{21,N_{\mathrm{n}}N_{\mathrm{p}}} & Z_{h-l}^{\mathrm{exp}}|^{\mathrm{uv}}_{21,N_{\mathrm{n}}N_{\mathrm{p}}} \\ Z_{h-l}^{\mathrm{exp}}|^{\mathrm{vu}}_{21,11} & Z_{h-l}^{\mathrm{exp}}|^{\mathrm{vv}}_{21,11} & Z_{h-l}^{\mathrm{exp}}|^{\mathrm{vu}}_{21,21} & Z_{h-l}^{\mathrm{exp}}|^{\mathrm{vv}}_{21,21} & \cdots & \cdots & Z_{h-l}^{\mathrm{exp}}|^{\mathrm{vu}}_{21,N_{\mathrm{n}}N_{\mathrm{p}}} & Z_{h-l}^{\mathrm{exp}}|^{\mathrm{vv}}_{21,N_{\mathrm{n}}N_{\mathrm{p}}} \\ \vdots & \vdots & \vdots & \vdots & \ddots & & \vdots & \vdots \\ \vdots & \vdots & \vdots & \vdots & & \ddots & \vdots & \vdots \\ Z_{h-l}^{\mathrm{exp}}|^{\mathrm{uu}}_{N_{\mathrm{n}}N_{\mathrm{p}},11} & Z_{h-l}^{\mathrm{exp}}|^{\mathrm{uv}}_{N_{\mathrm{n}}N_{\mathrm{p}},11} & Z_{h-l}^{\mathrm{exp}}|^{\mathrm{uu}}_{N_{\mathrm{n}}N_{\mathrm{p}},21} & Z_{h-l}^{\mathrm{exp}}|^{\mathrm{uv}}_{N_{\mathrm{n}}N_{\mathrm{p}},21} & \cdots & \cdots & Z_{h-l}^{\mathrm{exp}}|^{\mathrm{uu}}_{N_{\mathrm{n}}N_{\mathrm{p}},N_{\mathrm{n}}N_{\mathrm{p}}} & Z_{h-l}^{\mathrm{exp}}|^{\mathrm{uv}}_{N_{\mathrm{n}}N_{\mathrm{p}},N_{\mathrm{n}}N_{\mathrm{p}}} \\ Z_{h-l}^{\mathrm{exp}}|^{\mathrm{vu}}_{N_{\mathrm{n}}N_{\mathrm{p}},11} & Z_{h-l}^{\mathrm{exp}}|^{\mathrm{vv}}_{N_{\mathrm{n}}N_{\mathrm{p}},11} & Z_{h-l}^{\mathrm{exp}}|^{\mathrm{vu}}_{N_{\mathrm{n}}N_{\mathrm{p}},21} & Z_{h-l}^{\mathrm{exp}}|^{\mathrm{vv}}_{N_{\mathrm{n}}N_{\mathrm{p}},21} & \cdots & \cdots & Z_{h-l}^{\mathrm{exp}}|^{\mathrm{vu}}_{N_{\mathrm{n}}N_{\mathrm{p}},N_{\mathrm{n}}N_{\mathrm{p}}} & Z_{h-l}^{\mathrm{exp}}|^{\mathrm{vv}}_{N_{\mathrm{n}}N_{\mathrm{p}},N_{\mathrm{n}}N_{\mathrm{p}}} \end{bmatrix} \tag{8}$$

1) The E-MOT matrices $\mathbf{Z}_{h-l}^{\text{exp}} = \mathbf{0}$ for $h - l > \lfloor D_{\max}/(c\Delta t)\rfloor + T_{\max}$. Here, $T_{\max}$ is the order of Lagrange polynomials used for constructing $T(t)$, and $D_{\max}$ is the largest distance possible on S. Consequently, the number of $\mathbf{Z}_{h-l}^{\text{exp}}$, which is not completely zero, decreases with increasing Δt (for lower frequency excitations), whereas at the same time, they become denser matrices. For example, for $D_{\max}/(c\Delta t) < 1$, every nonzero $\mathbf{Z}_{h-l}^{\text{exp}}$ is a fully dense matrix. For smaller Δt (for higher frequency excitations), the opposite happens: the number of $\mathbf{Z}_{h-l}^{\text{exp}}$, which are not completely zero, increases, whereas, at the same time, they become sparser matrices.
2) $\mathbf{Z}_{h-l}^{\text{exp}}$ and $\mathbf{Z}_{h-l}^{\text{imp}}$ have the same sparsity structure since the entires of $\mathbf{G}$ contribute to entries of $\mathbf{Z}_{h-l}^{\text{imp}}$ when $\partial_t T(t)|_{t=(h-l)\Delta t} \neq 0$ and $\mathbf{r}_{jq} = \mathbf{r}_{ip}$ (test and source interpolation nodes are the same), and the entries of $\mathbf{Z}_{h-l}^{\text{exp}}$ are already nonzero for these cases.
3) Let $C_{\text{fix}}^{\text{exp}}$ and $C_{\text{fix}}^{\text{imp}}$ represent the cost of computing $\mathbf{V}_h^{\text{fix}} = \mathbf{V}_h^{\text{i}} - \sum_{l=1}^{h-1} \mathbf{Z}_{h-l}^{\text{exp}}\mathbf{I}_l$ [see (10)] by E-MOT and $\mathbf{V}_h^{\text{i}} - \sum_{l=1}^{h-1} \mathbf{Z}_{h-l}^{\text{imp}}\mathbf{I}_l$ [see the right-hand side of (15)] by I-MOT, respectively, at a given time step. Since the sparseness levels of $\mathbf{Z}_{h-l}^{\text{exp}}$ and $\mathbf{Z}_{h-l}^{\text{imp}}$ are the same (even though not all entries of these matrices are the same—see comment (ii) above), the cost of computing the summations $\sum_{l=1}^{h-1} \mathbf{Z}_{h-l}^{\text{exp}}\mathbf{I}_l$ and $\sum_{l=1}^{h-1} \mathbf{Z}_{h-l}^{\text{imp}}\mathbf{I}_l$ is the same, which means that $C_{\text{fix}}^{\text{exp}} = C_{\text{fix}}^{\text{imp}}$. Note that, regardless of Δt, the computation of $\sum_{l=1}^{h-1} \mathbf{Z}_{h-l}^{\text{exp}}\mathbf{I}_l$ or $\sum_{l=1}^{h-1} \mathbf{Z}_{h-l}^{\text{imp}}\mathbf{I}_l$ at any time step $h > \lfloor D_{\max}/(c\Delta t)\rfloor + T_{\max}$ requires $O(N_{\text{s}}^2)$ operations. Here, $N_{\text{s}} = 2N_{\text{p}}N_{\text{n}}$ is the number of unknowns. However, depending on Δt, cost of this computation relative to overall cost of E-MOT or I-MOT changes.

Let $C_{\text{tot}}^{\text{imp}} = C_{\text{sol}}^{\text{imp}} + C_{\text{fix}}^{\text{imp}}$ and $C_{\text{tot}}^{\text{exp}} = C_{\text{sol}}^{\text{exp}} + C_{\text{fix}}^{\text{exp}}$ denote the total computational cost per time step for I-MOT and E-MOT, respectively. Here, $C_{\text{sol}}^{\text{exp}}$ is the computational cost for Steps 2–4 of the PE(CE)^m method used by E-MOT and is obtained as

$$C_{\text{sol}}^{\text{exp}} \sim O(\{m[2K+1]+2K\}N_{\text{s}}) + O([m+1]\gamma N_{\text{s}}) + O([m+1]2N_{\text{s}})$$

where m is the number of corrector updates, and γ is defined as the average number of nonzero entries in rows of $\mathbf{Z}_0^{\text{exp}}$. The first term is the total cost of summations in Step 2 (once) and Step 4.1 (m times), respectively. The second term is the total cost of matrix-vector products $\mathbf{Z}_0^{\text{exp}}\mathbf{I}_h$ in Step 3 (once) and $\mathbf{Z}_0^{\text{exp}}\mathbf{I}_h^{(n)}$ in Step 4.2 (m times). The last term is the total cost of matrix-vector products involving $\mathbf{G}^{-1}$ in Step 3 (once) and Step 4.2 (m times).

I-MOT uses an iterative method to solve the matrix system (15). Let $C_{\text{sol}}^{\text{imp}}$ represent the cost of this solution

$$C_{\text{sol}}^{\text{imp}} \sim O\left(N_{\text{iter}}^{\text{imp}} F_{\text{iter}}^{\text{imp}} \gamma N_{\text{s}}\right)$$

where $N_{\text{iter}}^{\text{imp}}$ and $F_{\text{iter}}^{\text{imp}}$ are the numbers of iterations and matrix-vector products $\mathbf{Z}_0^{imp}\mathbf{I}_h^{(n)}$ carried out at every iteration, respectively. Note that $\mathbf{Z}_0^{\text{imp}}$ and $\mathbf{Z}_0^{\text{exp}}$ have the same γ [see comment (ii) above].

When $\Delta t \ll D_{\max}/c$ (high-frequency excitation), $\mathbf{Z}_0^{\text{exp}}$ and $\mathbf{Z}_0^{\text{imp}}$ are both very sparse, i.e., $\gamma \ll N_{\text{s}}$ (see comment (i) above). Therefore, $C_{\text{sol}}^{\text{imp}}$ and $C_{\text{sol}}^{\text{exp}}$ scale as $C_{\text{sol}}^{\text{imp}} \sim O(N_{\text{iter}}^{\text{imp}} F_{\text{iter}}^{\text{imp}} \gamma N_{\text{s}})$ and $C_{\text{sol}}^{\text{exp}} \sim O(mKN_{\text{s}}) + O(m\gamma N_{\text{s}})$, respectively. Comparing these estimates with $C_{\text{fix}}^{\text{exp}}$ and $C_{\text{fix}}^{\text{imp}}$ (see comment (iii) above), one can see that $C_{\text{sol}}^{\text{imp}} \ll C_{\text{fix}}^{\text{imp}}$ and $C_{\text{sol}}^{\text{exp}} \ll C_{\text{fix}}^{\text{exp}}$, which consequently results in $C_{\text{tot}}^{\text{imp}} \approx C_{\text{fix}}^{\text{imp}}$ and $C_{\text{tot}}^{\text{exp}} \approx C_{\text{fix}}^{\text{exp}}$, respectively. This means that both solvers have similar total execution times under high-frequency excitations as also shown by results presented in Section III.

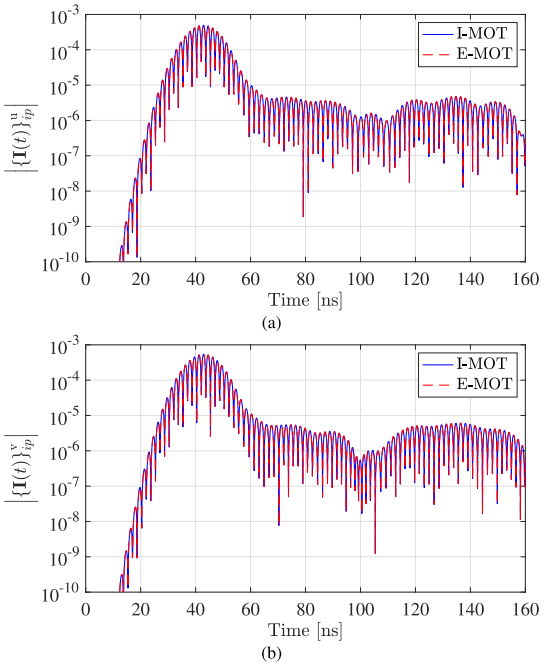

Fig. 1. (a) $|\{\mathbf{I}(t)\}_{ip}^{\text{u}}|$ and (b) $|\{\mathbf{I}(t)\}_{ip}^{\text{v}}|$, $p = 1014$, $i = 6$ calculated by the MOT schemes at $\mathbf{r}_{ip} = (0.97, -0.245, 0.005)$ m.

As the frequency of excitation decreases (for large Δt, $\Delta t \approx D_{\max}/c$), $\mathbf{Z}_0^{\text{exp}}$ and $\mathbf{Z}_0^{\text{imp}}$ become denser (and even full), resulting in $\gamma \approx N_{\text{s}}$ (see comments (i) above). Consequently, $C_{\text{sol}}^{\text{imp}} \sim O(N_{\text{iter}}^{\text{imp}} F_{\text{iter}}^{\text{imp}} N_{\text{s}}^2)$ and $C_{\text{sol}}^{\text{exp}} \sim O(mN_{\text{s}}^2)$ result in $C_{\text{fix}}^{\text{imp}} \ll C_{\text{sol}}^{\text{imp}}$ and $C_{\text{fix}}^{\text{exp}} \ll C_{\text{sol}}^{\text{exp}}$, respectively (see comment (iii) above). In summary, under low-frequency excitations, $C_{\text{tot}}^{\text{imp}} \approx C_{\text{sol}}^{\text{imp}}$ and $C_{\text{tot}}^{\text{exp}} \approx C_{\text{sol}}^{\text{exp}}$ and E-MOT is faster than I-MOT for $m < N_{\text{iter}}^{\text{imp}} F_{\text{iter}}^{\text{imp}}$. In Section III, it is shown by numerical results that this condition is satisfied.

It is well-known that $C_{\text{fix}}^{\text{imp}}$ can be reduced using PWTD [10]–[13] or FFT-based schemes [14]–[16]. However, the same algorithms can be applied to $C_{\text{fix}}^{\text{exp}}$ without any modifications, ensuring that $C_{\text{fix}}^{\text{exp}} = C_{\text{fix}}^{\text{imp}}$ would still hold. Similarly, FFT-based methods have been developed to reduce the cost of matrix-vector product $\mathbf{Z}_0^{\text{imp}}\mathbf{I}_h^{(n)}$ required by I-MOT [17]. E-MOT can utilize this method in the same way to compute the matrix-vector products $\mathbf{Z}_0^{\text{exp}}\mathbf{I}_h$ and $\mathbf{Z}_0^{\text{exp}}\mathbf{I}_h^{(n)}$.

III. Numerical Results

In this section, E-MOT and I-MOT are used to analyze transient electromagnetic scattering from a unit sphere centered at the origin. The sphere is excited by a planewave with magnetic field

$$\mathbf{H}^{\text{i}}(\mathbf{r}, t) = \hat{\mathbf{y}}\sqrt{\varepsilon/\mu}\, G(t - \hat{\mathbf{k}}\cdot\mathbf{r}/c) \tag{20}$$

where $\hat{\mathbf{k}} = \hat{\mathbf{z}}$ is the direction of propagation, and $G(t) = \cos[2\pi f_0(t-t_0)]e^{-(t-t_0)^2/(2w^2)}$ is a Gaussian pulse, where $w = 7/(2\pi f_{\text{bw}})$, f_{bw}, f_0, and $t_0 = 3.5w + 10/(f_0 + f_{\text{bw}})$ are the pulse duration, bandwidth, modulation frequency, and delay, respectively. Note that $f_{\max} = f_0 + f_{\text{bw}}$ is the effective maximum frequency. In all examples, the order of $\ell_{ip}(\mathbf{r})$ used by the Nyström method is two ($N_{\text{n}} = 6$) [21], and the order of Lagrange polynomials used for constructing $T(t)$ is three ($T_{\max} = 3$). The predictor coefficients $\mathbf{p}$ and the corrector coefficients $\mathbf{c}$ are obtained using the Adams–Bashforth and backward difference methods, respectively, resulting in $K = 4$ for the PE(CE)^m scheme [24]. Convergence thresholds for corrector updates and the TFQMR scheme are $\chi^{\text{PECE}} = \chi^{\text{TFQMR}} = 10^{-13}$.

For the first set of simulations, $N_{\text{p}} = 1126$ ($N_{\text{s}} = 13512$), $f_0 = 300$ MHz, $f_{\text{bw}} = 200$ MHz, $N_{\text{t}} = 1600$, and $\Delta t =$

TABLE I
EXECUTION TIMES OF THE MOT SCHEMES' DIFFERENT STAGES

		I-MOT					E-MOT						
N_s	f_0	$\sigma_{\text{err}}^{\text{imp}}$	$T_{\text{fix}}^{\text{imp}}$[s]	$T_{\text{TFQMR}}^{\text{imp}}$[s]	$T_{\text{tot}}^{\text{imp}}$[s]	$\{N_{\text{iter}}^{\text{imp}} F_{\text{iter}}^{\text{imp}}\}_{\text{avg}}$	$\sigma_{\text{err}}^{\text{exp}}$	$T_{\text{fix}}^{\text{exp}}$[s]	$T_{\text{PECE}}^{\text{exp}}$[s]	$T_{\text{tot}}^{\text{exp}}$[s]	m_{avg}	$\frac{T_{\text{TFQMR}}^{\text{imp}}}{T_{\text{PECE}}^{\text{exp}}}$	$\frac{T_{\text{tot}}^{\text{imp}}}{T_{\text{tot}}^{\text{exp}}}$
2424	5	0.011	61.81	763.61	825.53	66.66	0.011	65.43	129.02	194.56	9.78	5.92	4.24
2424	10	0.007	67.67	567.24	635.00	68.02	0.007	68.05	67.68	135.83	7.19	8.38	4.68
2424	25	0.004	83.87	100.29	184.21	70.15	0.004	83.65	7.40	91.14	4.19	13.55	2.02
2424	50	0.025	89.84	55.09	144.99	80.26	0.025	90.02	3.46	93.57	3.92	15.92	1.55
2424	100	0.047	91.70	28.56	120.31	92.53	0.047	91.71	2.07	93.86	5.20	13.80	1.28
2424	200	0.046	93.85	19.52	113.41	96.40	0.046	93.99	1.33	95.42	4.77	14.68	1.19
2424	400	0.068	99.47	8.61	108.13	99.80	0.068	99.62	0.63	100.33	4.32	13.67	1.08
7464	5	0.010	583.40	6266.59	6850.92	57.62	0.010	585.11	1155.56	1741.13	9.79	5.42	3.93
7464	10	0.006	638.02	4650.56	5289.34	58.56	0.006	637.91	640.10	1278.45	7.20	7.27	4.14
7464	25	0.004	779.17	784.12	1563.65	60.78	0.004	780.93	64.87	846.22	4.06	12.09	1.85
7464	50	0.025	828.96	349.04	1178.32	70.56	0.025	829.76	22.90	853.07	3.56	15.24	1.38
7464	100	0.047	850.05	136.80	987.14	79.08	0.047	851.62	10.80	862.83	4.85	12.67	1.14
7464	200	0.046	857.49	69.68	927.46	81.46	0.046	851.57	5.59	857.57	4.68	12.47	1.08
7464	400	0.066	882.09	44.40	926.77	82.91	0.066	884.64	3.70	888.75	4.46	12.00	1.04

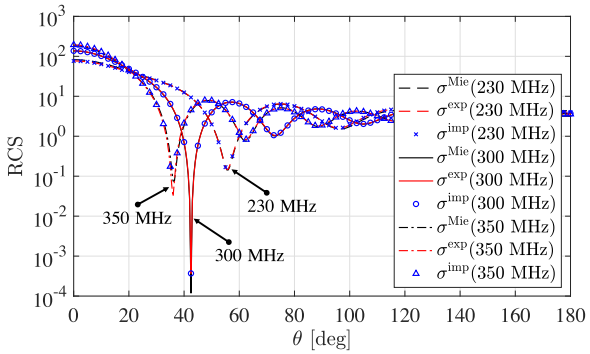

Fig. 2. $\sigma^{\text{Mie}}(\theta, \varphi, f)$, $\sigma^{imp}(\theta, \varphi, f)$, and $\sigma^{exp}(\theta, \varphi, f)$ versus θ for $\varphi = 0°$ and $f \in \{230, 300, 350\}$ MHz.

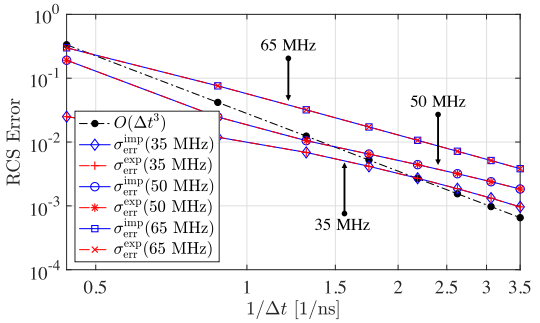

Fig. 3. L_2-norm error in RCS obtained from the solutions computed by the MOT schemes versus $1/\Delta t$.

0.1 ns $[1/(20 f_{\max})]$. Fig. 1(a) and (b) shows the comparison of $|\{\mathbf{I}(t)\}_{ip}^{\text{u}}|$ and $|\{\mathbf{I}(t)\}_{ip}^{\text{v}}|$ computed by I-MOT and E-MOT at $\mathbf{r}_{ip} = (0.97, -0.245, 0.005)$ m ($p = 1014$, $i = 6$), respectively. The results agree very well.

Let $\sigma^{\text{Mie}}(\theta, \varphi, f)$, $\sigma^{\text{imp}}(\theta, \varphi, f)$, and $\sigma^{\text{exp}}(\theta, \varphi, f)$ denote the radar cross section (RCS) values computed using the Mie series solution and the Fourier transform of the solutions obtained by I-MOT and E-MOT, respectively. Fig. 2 shows the plots of $\sigma^{\text{Mie}}(\theta, \varphi, f)$, $\sigma^{imp}(\theta, \varphi, f)$, and $\sigma^{exp}(\theta, \varphi, f)$ versus θ for $\varphi = 0°$ and $f \in \{230, 300, 350\}$ MHz. The figure clearly shows that the solutions obtained by I-MOT and E-MOT are accurate within the band of the excitation.

For the second set of simulations, two spatial discretizations are considered: $N_{\text{p}} = 202$ ($N_{\text{s}} = 2424$) and $N_{\text{p}} = 622$ ($N_{\text{s}} = 7464$). For each discretization, seven sets of excitations are considered: $f_0 = \{5, 10, 25, 50, 100, 200, 400\}$ MHz and $f_{\text{bw}} = 0.75 f_0$. E-MOT and I-MOT are both executed for $N_{\text{t}} = 500$ time steps with $\Delta t = 1/(17.5 f_0) = 1/(10 f_{\max})$. The "denseness" level in $\mathbf{Z}_0^{\text{exp}}$ and $\mathbf{Z}_0^{\text{imp}}$ for these values of Δt and two different discretizations are $\gamma = \{2424, 1777, 303, 143, 61, 38, 13\}$ for $N_{\text{p}} = 202$ and $\gamma = \{7464, 5471, 881, 340, 116, 54, 32\}$ for $N_{\text{p}} = 622$, respectively. For each excitation and discretization, RCS values $\sigma^{\text{imp}}(\theta, \varphi, f)$ and $\sigma^{\text{exp}}(\theta, \varphi, f)$ are computed for $\theta = [0°, 180°]$, $\varphi = 0°$, and $f = f_0$ using the Fourier transform of the solutions obtained by I-MOT and E-MOT, respectively. The L_2-norm error in RCS is defined as

$$\sigma_{\text{err}}^{\text{type}} = \sqrt{\frac{\sum_{n=0}^{360} |\sigma^{\text{type}}(n\Delta\theta, \varphi, f) - \sigma^{\text{Mie}}(n\Delta\theta, \varphi, f)|^2}{\sum_{n=0}^{360} |\sigma^{\text{Mie}}(n\Delta\theta, \varphi, f)|^2}} \quad (21)$$

where type $\in \{\text{imp}, \text{exp}\}$, $f = f_0$, $\Delta\theta = 0.5°$, and $\varphi = 0°$. Table I shows $\sigma_{\text{err}}^{\text{imp}}$ and $\sigma_{\text{err}}^{\text{exp}}$ and shows that the error level in the solutions obtained by I-MOT and E-MOT is the same.

The execution times of the different stages of MOT schemes are compared in Table I. Here, $T_{\text{fix}}^{\text{imp}}$ and $T_{\text{fix}}^{\text{exp}}$ are the total times required for computing $\mathbf{V}_h^{\text{i}} - \sum_{l=1}^{h-1} \mathbf{Z}_{h-l}^{\text{imp}} \mathbf{I}_l$ and $\mathbf{V}_h^{\text{i}} - \sum_{l=1}^{h-1} \mathbf{Z}_{h-l}^{\text{exp}} \mathbf{I}_l$ for $h = 1, \ldots, N_{\text{t}}$, by I-MOT and E-MOT, respectively. $T_{\text{TFQMR}}^{\text{imp}}$ is the total time required to iteratively solve the I-MOT system in (15) by the TFQMR method for $h = 1, \ldots, N_{\text{t}}$. $T_{\text{PECE}}^{\text{exp}}$ is the total time required by the PE(CE)^m method for $h = 1, \ldots, N_{\text{t}}$. $T_{\text{tot}}^{\text{imp}}$ and $T_{\text{tot}}^{\text{exp}}$ are the total execution times of I-MOT and E-MOT, respectively. Finally, $\{N_{\text{iter}}^{\text{imp}} F_{\text{iter}}^{\text{imp}}\}_{\text{avg}}$ and m_{avg} are the average values of $N_{\text{iter}}^{\text{imp}} F_{\text{iter}}^{\text{imp}}$ and m over N_{t} time steps, respectively.

Table I shows that, as expected, $T_{\text{fix}}^{\text{imp}}$ and $T_{\text{fix}}^{\text{exp}}$ are almost the same. Furthermore, for all values of Δt, $T_{\text{PECE}}^{\text{exp}} < T_{\text{TFQMR}}^{\text{imp}}$ since $m_{\text{avg}} \ll \{N_{\text{iter}}^{\text{imp}} F_{\text{iter}}^{\text{imp}}\}_{\text{avg}}$. This has different consequences for simulations with large and small Δt. For large Δt (low-frequency excitation), $T_{\text{TFQMR}}^{\text{imp}} \gg T_{\text{fix}}^{\text{imp}}$, $T_{\text{PECE}}^{\text{exp}} \gg T_{\text{fix}}^{\text{exp}}$, and $T_{\text{fix}}^{\text{imp}} \approx T_{\text{fix}}^{\text{exp}}$, therefore, $T_{\text{tot}}^{\text{imp}} > T_{\text{tot}}^{\text{exp}}$. Indeed, the results show that the E-MOT is roughly four times faster than I-MOT. As Δt gets smaller (frequency gets higher), $T_{\text{fix}}^{\text{imp}}$ and $T_{\text{fix}}^{\text{exp}}$ become larger than $T_{\text{TFQMR}}^{\text{imp}}$ and $T_{\text{PECE}}^{\text{exp}}$, and the fact that $T_{\text{PECE}}^{\text{exp}} < T_{\text{TFQMR}}^{\text{imp}}$ does not reflect on the total MOT times $T_{\text{tot}}^{\text{exp}}$ and $T_{\text{tot}}^{\text{imp}}$ anymore. Indeed, the results show that both schemes require almost the same time to complete the simulations as Δt gets smaller. The CPU times shown in Table I confirm the computational complexity analysis in Section II-F.

For the last set of simulations, $N_p = 622$ ($N_s = 7464$), $f_0 = 50$ MHz, and $f_{bw} = 37.5$ MHz, and I-MOT and E-MOT are executed for the different values of Δt changed between 2.29 ns $[1/(5f_{max})]$ and 0.29 ns $[1/(40f_{max})]$. RCS L_2-norm error values σ_{err}^{imp} and σ_{err}^{exp} are computed for $f \in \{35, 50, 65\}$ MHz, $\Delta\theta = 0.5°$, and $\varphi = 0°$ using (21). Fig. 3 shows the plots of σ_{err}^{imp} and σ_{err}^{exp} versus $1/\Delta t$ for $f \in \{35, 50, 65\}$ MHz. This figure clearly shows that E-MOT has the same accuracy as I-MOT (as discussed in Section II-E). In addition, Fig. 3 shows that the accuracy of the schemes follows the convergence curve of $O(\Delta t^3)$ for larger values of Δt (note that the order of Lagrange polynomials constructing $T(t)$ is $T_{max} = 3$), but, for the smaller values of Δt, the accuracy is limited by the second-order spatial discretization, and as a result, the convergence with respect to $1/\Delta t$ becomes slightly slower than $O(\Delta t^3)$.

IV. Conclusion

An explicit MOT scheme to efficiently solve the TD-MFIE for large time step sizes (under low-frequency excitations) is developed. The current is spatially expanded using high-order nodal functions defined on curvilinear triangles discretizing the scatterer surface. Applying Nyström discretization, which uses this expansion, to the TD-MFIE yields a system of ODEs in time-dependent expansion coefficients. This system is integrated in time using a PE(CE)^m method to compute the samples of these coefficients. The Gram matrix arising from the Nyström discretization is block-diagonal with 2×2 blocks, and its inverse is constructed from the inverse of the blocks before the time marching. Therefore, the matrix inversion needed at each time step is replaced by the product of the inverse block-diagonal Gram matrix and the right-hand side vector. Numerical results show that the resulting MOT scheme can use the time step sizes as large as those would be used by its implicit counterpart without sacrificing the stability, has the same level of accuracy, and is more than four times faster for low-frequency excitations.

The explicit MOT scheme can be extended to solve the TD-CFIE obtained by combining the TD-MFIE with the Calderón-preconditioned TD-EFIE. The Calderón-preconditioning ensures that the TD-CFIE is a second-kind surface integral equation [26]–[29].

References

[1] B. P. Rynne and P. D. Smith, "Stability of time marching algorithms for the electric field integral equation," *J. Electromagn. Waves Appl.*, vol. 4, no. 12, pp. 1181–1205, Jan. 1990.

[2] M. J. Bluck and S. P. Walker, "Time-domain BIE analysis of large three-dimensional electromagnetic scattering problems," *IEEE Trans. Antennas Propag.*, vol. 45, no. 5, pp. 894–901, May 1997.

[3] G. Manara, A. Monorchio, and R. Reggiannini, "A space-time discretization criterion for a stable time-marching solution of the electric field integral equation," *IEEE Trans. Antennas Propag.*, vol. 45, no. 3, pp. 527–532, Mar. 1997.

[4] F. P. Andriulli, H. Bagci, F. Vipiana, G. Vecchi, and E. Michielssen, "A marching-on-in-time hierarchical scheme for the solution of the time domain electric field integral equation," *IEEE Trans. Antennas Propag.*, vol. 55, no. 12, pp. 3734–3738, Dec. 2007.

[5] A. Dely, F. P. Andriulli, and K. Cools, "Large time step and DC stable TD-EFIE discretized with implicit Runge–Kutta methods," *IEEE Trans. Antennas Propag.*, vol. 68, no. 2, pp. 976–985, Feb. 2020.

[6] Y. Beghein, K. Cools, H. Bagci, and D. De Zutter, "A space-time mixed Galerkin marching-on-in-time scheme for the time-domain combined field integral equation," *IEEE Trans. Antennas Propag.*, vol. 61, no. 3, pp. 1228–1238, Mar. 2013.

[7] A. J. Pray, Y. Beghein, N. V. Nair, K. Cools, H. Bagci, and B. Shanker, "A higher order space-time Galerkin scheme for time domain integral equations," *IEEE Trans. Antennas Propag.*, vol. 62, no. 12, pp. 6183–6191, Dec. 2014.

[8] H. A. Ulku, H. Bagci, and E. Michielssen, "Marching on-in-time solution of the time domain magnetic field integral equation using a predictor-corrector scheme," *IEEE Trans. Antennas Propag.*, vol. 61, no. 8, pp. 4120–4131, Aug. 2013.

[9] R. Chen and H. Bagci, "An explicit MOT scheme for solving the Nyström-discretized TD-MFIE," in *Proc. IEEE Int. Symp. Antennas Propag. USNC/URSI Nat. Radio Sci. Meeting*, Jul. 2018, pp. 2443–2444.

[10] B. Shanker, A. A. Ergin, K. Aygun, and E. Michielssen, "Analysis of transient electromagnetic scattering from closed surfaces using a combined field integral equation," *IEEE Trans. Antennas Propag.*, vol. 48, no. 7, pp. 1064–1074, Jul. 2000.

[11] B. Shanker, A. A. Ergin, M. Lu, and E. Michielssen, "Fast analysis of transient electromagnetic scattering phenomena using the multilevel plane wave time domain algorithm," *IEEE Trans. Antennas Propag.*, vol. 51, no. 3, pp. 628–641, Mar. 2003.

[12] Y. Liu, A. C. Yucel, H. Bagci, and E. Michielssen, "A scalable parallel PWTD-accelerated SIE solver for analyzing transient scattering from electrically large objects," *IEEE Trans. Antennas Propag.*, vol. 64, no. 2, pp. 663–674, Feb. 2016.

[13] K. Aygun, B. Shanker, A. A. Ergin, and E. Michielssen, "A two-level plane wave time-domain algorithm for fast analysis of EMC/EMI problems," *IEEE Trans. Electromagn. Compat.*, vol. 44, no. 1, pp. 152–164, Feb. 2002.

[14] H. Bagci, A. E. Yilmaz, V. Lomakin, and E. Michielssen, "Fast solution of mixed-potential time-domain integral equations for half-space environments," *IEEE Trans. Geosci. Remote Sens.*, vol. 43, no. 2, pp. 269–279, Feb. 2005.

[15] H. Bagci, A. E. Yilmaz, J.-M. Jin, and E. Michielssen, "Fast and rigorous analysis of EMC/EMI phenomena on electrically large and complex cable-loaded structures," *IEEE Trans. Electromagn. Compat.*, vol. 49, no. 2, pp. 361–381, May 2007.

[16] A. E. Yilmaz, J.-M. Jin, and E. Michielssen, "Time domain adaptive integral method for surface integral equations," *IEEE Trans. Antennas Propag.*, vol. 52, no. 10, pp. 2692–2708, Oct. 2004.

[17] A. E. Yilmaz, J.-M. Jin, and E. Michielssen, "Analysis of low-frequency electromagnetic transients by an extended time-domain adaptive integral method," *IEEE Trans. Adv. Packag.*, vol. 30, no. 2, pp. 301–312, May 2007.

[18] J. Cao, R. S. Chen, Y. Hu, and S. Tao, "A higher order Nyström scheme for a marching-on-in-time solution of time-domain integral equation," *IEEE Trans. Antennas Propag.*, vol. 63, no. 6, pp. 2762–2767, Mar. 2015.

[19] S. Rao, D. Wilton, and A. Glisson, "Electromagnetic scattering by surfaces of arbitrary shape," *IEEE Trans. Antennas Propag.*, vol. AP-30, no. 3, pp. 409–418, May 1982.

[20] R. Chen, S. B. Sayed, N. Alharthi, D. Keyes, and H. Bagci, "An explicit marching-on-in-time scheme for solving the time domain kirchhoff integral equation," *J. Acoust. Soc. Amer.*, vol. 146, no. 3, pp. 2068–2079, Sep. 2019.

[21] G. Kang, J. Song, W. Cho Chew, K. C. Donepudi, and J.-M. Jin, "A novel grid-robust higher order vector basis function for the method of moments," *IEEE Trans. Antennas Propag.*, vol. 49, no. 6, pp. 908–915, Jun. 2001.

[22] S. B. Sayed, H. Arda Ulku, and H. Bagci, "Explicit time marching schemes for solving the magnetic field volume integral equation," *IEEE Trans. Antennas Propag.*, vol. 68, no. 3, pp. 2224–2237, Mar. 2020.

[23] M. G. Duffy, "Quadrature over a pyramid or cube of integrands with a singularity at a vertex," *SIAM J. Numer. Anal.*, vol. 19, no. 6, pp. 1260–1262, Dec. 1982.

[24] E. Hairer, S. P. Norsett, and G. Wanner, *Solving Ordinary Differential Equations I: Nonstiff Problems*. New York, NY, USA: Springer-Verlag, 1991.

[25] R. W. Freund, "A transpose-free quasi-minimal residual algorithm for non-hermitian linear systems," *SIAM J. Scientific Comput.*, vol. 14, no. 2, pp. 470–482, Mar. 1993.

[26] H. Bagci, F. P. Andriulli, K. Cools, F. Olyslager, and E. Michielssen, "A Calderón multiplicative preconditioner for the combined field integral equation," *IEEE Trans. Antennas Propag.*, vol. 57, no. 10, pp. 3387–3392, Oct. 2009.

[27] H. A. Ulku, H. Bagci, and E. Michielssen, "Explicit solution of Calderon preconditioned time domain integral equations," in *Proc. IEEE Antennas Propag. Soc. Int. Symp. (APSURSI)*, Jul. 2013, pp. 39–40.

[28] K. Cools, F. P. Andriulli, F. Olyslager, and E. Michielssen, "Time domain CalderÓn identities and their application to the integral equation analysis of scattering by PEC objects Part I: Preconditioning," *IEEE Trans. Antennas Propag.*, vol. 57, no. 8, pp. 2352–2364, Aug. 2009.

[29] F. P. Andriulli, K. Cools, F. Olyslager, and E. Michielssen, "Time domain CalderÓn identities and their application to the integral equation analysis of scattering by PEC objects Part II: Stability," *IEEE Trans. Antennas Propag.*, vol. 57, no. 8, pp. 2365–2375, Aug. 2009.